

SYNTHESIS AND CHARACTERIZATION OF CdS/UiO-66/Ag₃PO₄ NANOCOMPOSITE FOR PHOTOCATALYTIC DEGRADATION OF METHYL ORANGE UNDER VISIBLE LIGHT IRRADIATION

Tesfahun Kebede*, Abi M. Tadesse and Beyenech Ergedo

Haramaya University, College of Natural and Computational Sciences, Department of
Chemistry, P.O. Box 138, Dire Dawa, Ethiopia

(Received September 24, 2020; Revised December 6, 2020; Accepted December 14, 2020)

ABSTRACT. Single, binary and ternary nanomaterials were synthesized by precipitation, solvothermal, simple solution and impregnation methods to serve as photocatalysts. The crystal structure, morphology, band gap energy, functional groups and optical properties of these materials were characterized by XRD, SEM-EDX, UV-Vis, FTIR, and PL instrumental techniques, respectively. Photocatalytic degradation performances of all the synthesized photocatalysts were investigated under visible light irradiation using MO as a model organic pollutant. The photocatalytic degradation performances of all the photocatalysts were evaluated on aqueous solution of the model pollutant dye as well as on a real sewage sample solution collected from Bahir Dar Textile Share Company. Results suggested that the optimized ternary nanocomposite photocatalyst exhibited a relatively higher efficiency towards the photodegradation of both the methyl orange (MO) dye solution (90%) and the real sewage sample solution (71.2%). The effect of operational parameters such as pH (4), initial dye concentration (10 mg/L) and photocatalyst load (0.2 g/L) in MO dye degradation were investigated by using the ternary CdS/UiO-66/Ag₃PO₄ (R₄) nanocomposite.

KEY WORDS: Metal-organic frameworks, Nanocomposite, Ternary system, Photocatalysts, Methyl orange

INTRODUCTION

Water contamination by organic pollutants such as dyes is a serious environmental problem for human society. In addition, dyed (colored) wastewater usually consists of a number of contaminants including acids, bases, dissolved solids, toxic compounds, and other colored materials [1]. Many dyes are considered to be toxic and even carcinogenic [2]. Dye contaminated wastewaters mostly enter the environment as discharges from textile, leather, paper, printing, plastic, and food industries [3]. The presence of small amounts of dyes in water (even < 1 mg/L) is highly visible; hence it affects the pleasant appearance and causes significant loss in luminosity apart from depletion of oxygen in the aquatic system [4]. Thus, the presence of dye materials greatly influences the quality of water and the removal of these kinds of pollutants from the environment is indispensable [5].

In the past decades, various physical, chemical, and biological techniques have been developed to remove organic pollutants from wastewater. Among these efforts, semiconductor based photodegradation is seen as one of the most advantageous strategies since organic pollutants can be directly degraded by this method [6-8]. Particularly, the photocatalysis process promoted by visible-light irradiation is more appealing due to its effective utilization of the solar energy [9, 10]. Metal oxides such as Fe₂O₃ and Ag₃PO₄ as well as metal sulfides like CdS have been studied as efficient photocatalysts for the degradation of various organics [11]. Most importantly, porous solids based heterogeneous photocatalytic technology has been developed recently as a much better solution to this challenge. In this regard, metal organic frameworks (MOFs) have attracted attention as catalysts in the degradation of dyes under light irradiation owing to their high surface areas, high porosity, high thermal stability, low density and

*Corresponding author. E-mail: tesfakhic@gmail.com

This work is licensed under the Creative Commons Attribution 4.0 International License

adjustable chemical functionalities [12]. More recently, MOFs that can act as photocatalysts have drawn much attention as the most fascinating materials for exploiting them in other new applications such as in the areas of separation, chemical sensing, gas storage, catalysis, biomedicine, etc., by exploiting their outstanding properties [13, 14]. In one of the pioneer works, MOF-5 and $Zn_3(\text{BTC})_2$ films were investigated for the photocatalytic degradation of organic dyes [15]. Unfortunately, most MOFs are wide band gap limited to the small portion of the solar spectrum. To address this problem, the focus of research has nowadays been placed on modifying this aspect of MOFs so as to make it possible for the MOFs to harness visible-light efficiently in photocatalytic activity. To overcome this problem, other semiconductor functional materials with photocatalytic activity can be immobilized on MOF substrate to obtain enhanced catalytic activity and improved stability. For example, it was found that MIL-88A and a series of MIL-53 MOFs (MIL-53(Fe) and MIL-53(Cr)) could be made effective photocatalysts in decomposing MB under visible-light irradiation [15]. In another case, some functional compounds were embedded on MIL-101 for visible-light driven H_2 production [16]. In a typical work, $\text{Cu}_3(\text{BTC})_2$ was formed as a core-shell structure along with TiO_2 , and the resulting composite was used as a platform to photocatalyze gaseous reactions [17]. In all these examples, the MOF supported semiconductor composites exhibited enhanced photocatalytic activities relative to those of the unsupported semiconductor materials.

Among various types of MOFs, UiO-66 has attracted attention for it possesses excellent properties and exhibits higher thermal and chemical stabilities; it has been researched extensively in the fields of catalysis, hydrogen generation, gas storage, drug delivery, etc. [18, 19]. In the recently published studies on UiO-66 based visible-light photocatalytic applications, UiO-66 was modified with various functional groups or used as a stable substrate to be coupled with different functional materials for H_2 production, CO_2 reduction, or organic compounds oxidation [19]. However, there are limited reports on UiO-66 based composite photocatalyst particularly for water treatment applications [19-21]. In this connection, UiO-66 incorporated with Ag_3PO_4 and CdS for photocatalytic application has not been reported yet. In this work, CdS/UiO-66/ Ag_3PO_4 composite was prepared by impregnation method and after characterization; the photocatalytic activity of this composite material was evaluated by conducting photodegradation studies using methyl orange as a model organic dye pollutant under visible-light irradiation.

EXPERIMENTAL

Instruments

Various types of instruments were used for the synthesis, characterization and photocatalytic experiments, which include: X-ray diffractometer (XRD) was used to record the phase formation of all the materials using X'Pert Pro PANalytical equipped with an X-ray source of a $\text{CuK}\alpha$ radiation (wavelength of 0.15406 nm) at step scan rate of 0.02 (step time: 1 s; 2θ range: 5.0-90.4). SEM-EDX (Hitachi TM1000) was used to determine morphology of the as-synthesized nanocomposites. UV/Vis spectrophotometer (SANYO, SP65, UK) was used for the determination of the absorption edge of the prepared samples. PL (RF 5301PC Shimadzu) and FTIR (Spectrum 65, PerkinElmer) were also used in the analysis of the as-synthesized photocatalysts.

Chemicals and reagents

All chemicals were of analytical grade (Sigma-Aldrich) and used as received. Zirconium oxychloride octahydrate salt, ($\text{ZrOCl}_2 \cdot 8\text{H}_2\text{O}$), 1,4-benzendicarboxylic acid or terephthalic acid, (BDC), silver nitrate (AgNO_3), Na_2HPO_4 , cadmium acetate tetra hydrate [$\text{Cd}(\text{CH}_3\text{COO})_2 \cdot 4\text{H}_2\text{O}$] and sodium sulfide nonahydrate ($\text{Na}_2\text{S} \cdot 9\text{H}_2\text{O}$) were used as the precursors of CdS, UiO-66,

Ag₃PO₄ and also NaNO₃, NaOH, HCl, NaHCO₃, CH₃OH/H₂O, methanol, ethanol, DMF and DMSO were used. Methyl orange was used as a model organic contaminant for investigating the photocatalytic activities of the as-synthesized photocatalysts.

Synthesis methods of nanocomposites

Single system nanoparticles (Zr-UiO-66-DMF, Ag₃PO₄ and CdS)

3.91 g/12.14 mmol of zirconium oxychloride octahydrate (ZrOCl₂.8H₂O) salt was dissolved in 50 mL of DMF and stirred for 30 min. Then 2.01 g/12.26 mmol of 1,4-benzendicarboxylic acid was dissolved in 50 mL of DMF and stirred for 30 min. The metal salt solution was added to the linker solution slowly and stirred for 24 h. The process continued for 24 h in an oven at 120 °C for a precipitation to form. The precipitate so formed was centrifuged at 2500 rpm for 30 min and the solid part was washed three times with DMF and four times with methanol. Finally, the solid [S₁] was dried in open air at room temperature and weighed [22]. It is expected to have structural formula of Zr₆O₄(OH)₄[C₆H₄(CO₂)₂]₁₂ [18]. Silver orthophosphate (Ag₃PO₄) was prepared by chemical precipitation method in the dark using silver nitrate and disodium hydrogen phosphate as raw materials [23]. To this effect first, a solution of AgNO₃ was prepared by adding 30 mmol/5.1 g of AgNO₃ powder in 150 mL deionized water. Likewise, a solution of Na₂HPO₄ was prepared by dissolving 10 mmol/1.42 g of Na₂HPO₄ powder in 100 mL deionized water. Then after, AgNO₃ solution was added drop by drop into the Na₂HPO₄ solution with continuous stirring for 3 h in the dark room and the precipitation so generated was made to settle down for 12 h. The resulting precipitate was filtered from the mother liquor and washed with double deionized water four times followed by ethanol two times. It was then dried at 60 °C for 12 h, and finally calcined at 300 °C for 2 h to get Ag₃PO₄ nanoparticles labeled as S₂. In this study, we have used cadmium acetate tetra hydrate (Cd(CH₃COO)₂.4H₂O) as a Cd⁺² ion source and disodium sulfide nanohydrate (Na₂S.9H₂O) as S⁻² ion source, respectively. For the synthesis of CdS nanoparticle using precipitation method, equal molarities of 0.1 M/12.78 g/41.4 mmol of Cd(CH₃COO)₂.4H₂O and 9.95 g/41.4 mmol of Na₂S.9H₂O solution were prepared in separate beakers. Then the sodium sulfide solution was added drop wise into the cadmium acetate solution with a continuous stirring for 2 h at room temperature to form a clear solution. During the reaction N₂ gas was continuously purged through the suspension. Then the resulting yellow precipitate was collected by centrifugation and washed three times with deionized water and ethanol to remove the residue. Finally, the obtained CdS precipitate was further dried at 70 for 5 h [24]. The clean solid precipitate was calcined at 300 °C for 2 h in a furnace, ground into powder and kept in a container by labeling it as CdS nanoparticle; S₃.

Binary nanocomposites (Ag₃PO₄/UiO-66, CdS/UiO-66 and CdS/UiO-66/Ag₃PO₄)

Ag₃PO₄/UiO-66 nanocomposite was prepared by a simple solution method based on methods described in [20] with some modifications. The Ag₃PO₄/UiO-66 composite was prepared based on the molar ratio of Ag:Zr. Typically, for the preparation of Ag₃PO₄/UiO-66 composite with Ag:Zr molar ratio of (0.5:1), 4.36 mg/0.0307 mmol of Na₂HPO₄ was dissolved in 9.5 mL of deionized water. Then after, 3.564 g/0.5474 mmol of the as synthesized UiO-66 were added to the Na₂HPO₄ solution. After stirring for 1 h, 15.64 mg/0.092 mmol of AgNO₃ dissolved in 28.48 mL of deionized water was added to the UiO-66 mixture drop wise. The total reaction mixture was about 38 mL in volume, and was stirred vigorously at room temperature for 12 h. Finally, the product was collected by filtration, thoroughly washed with deionized water for several times, and dried in vacuum oven at 80 °C (B₁).

CdS/UiO-66 nanocomposite was prepared following the procedure described by [21]. Accordingly, 0.133 g/0.45 mmol of Cd(CH₃COO)₂.4H₂O and 0.5 g/1.55 mmol of the as-synthesized UiO-66 were dissolved in 50 mL DMSO/dimethyl sulfoxide/(CH₃)₂SO. After

magnetic stirring for 60 min, the obtained suspension was placed in an oven and heated to 180 °C for 12 h. The reaction mixture was cooled to room temperature. The products were collected and rinsed through centrifugation followed by redispersion processes using water and ethanol three times. The CdS loaded UiO-66 hybrids were obtained after drying the washed powders in vacuum oven overnight at 80 °C (B₂). For the synthesis of CdS/Ag₃PO₄ nanostructures (Ag₃PO₄/CdS ratio of 3), 2.07 mmol/0.3 g of CdS nanoparticles was dispersed in 50 mL of deionized water and stirred for 2 h. To the above dispersion 6.21 mmol/2.37 g of Na₂HPO₄ was added with vigorous stirring for 1 h. Finally, 18.63 mmol/3.16 g of Ag₃PO₄ was added to the reaction mixture. Formation of the composite material proceeded for 2 h at room temperature at pH of 4. The resulting yellowish precipitate was dried for 12 h in a vacuum oven and calcined at 300 °C for 3 h (B₃) [25].

Ternary nanocomposite CdS /UiO-66/Ag₃PO₄

For the preparation of the ternary nanocomposite CdS/Ag₃PO₄/UiO-66, we varied the Ag to Cd mole ratios to 1, 2, 3 and 4 keeping the amount of Ag₃PO₄/UiO-66 binary system fixed. In a typical synthesis, 3 g/0.4328 mmol of the Ag₃PO₄/UiO-66 binary composite was dispersed in 50 mL of deionized water and sonicated for 2 h. Similarly, different molar ratios of the precursor of CdS nanoparticle (Cd(CH₃COO)₂·4H₂O and Na₂S·9H₂O) were dissolved in deionized water. A solution of certain amount of the [Cd(OAC)₂·4H₂O] (1.54, 2.06, 3.06 and 6.10 mg, corresponding to Ag/Cd mole ratio of 4, 3, 2, and 1) was added to the above dispersion and sonicated further for 2 h. Finally, stoichiometric amount of Na₂S·9H₂O (1.20, 1.61, 2.40 and 4.75 mg) dissolved in 50 mL of DIW was added to the above mixture and stirred vigorously for 1 h. The precipitate obtained as such was filtered and washed four times by deionized water (DIW) and two times with ethanol to remove impurity. The product was dried at 80 °C for 12 h in vacuum oven. The obtained powder was then ground to get fine particles and then labeled as R₁, R₂, R₃ and R₄ for each molar ratios (1:1, 2:1, 3:1 and 4:1), respectively.

Photocatalytic activity

Photocatalytic activities of the as-synthesized photocatalysts were studied through comparison of methyl orange (MO) degradation under dark and visible light using each of the as-synthesized photocatalysts at a time. For studying the methyl orange degradation, 0.2 g/L of each as-synthesized photocatalyst powder and 10 mg/L of 100 mL aqueous solution of MO was taken in a reactor tube. The suspension of catalyst and MO may be expected to achieve adsorption-desorption equilibration after the reactor was kept for 1 h under dark environment [26]. Then the suspension was subjected to visible light irradiation with continuous stirring using a magnetic stirrer. In the event of doing the stirring air/oxygen was purged into the solution as required. Then absorbance of MO aqueous solution was measured in 20 min time interval by taking each time 10 mL of the solution. In other words, 10 mL the MO aqueous suspension was withdrawn at 20 min time interval, centrifuged at 3000 rpm for 10 min and then filtered off; the clear solution was taken in cuvette and its absorbance measured at λ_{max} of MO. The percentage degradation was calculated for each case using the formula:

$$\% \text{ Degradation} = \frac{A_0 - A_t}{A_0} \times 100 \quad (1)$$

where A₀ is absorbance of dye at initial stage, A_t is absorbance of dye at time “t”.

Rate of degradation of methyl orange by the photocatalysts was expressed by the Langmuir-Hinshelwood model. When the initial concentration of the dye is lower, the reaction rate can be expressed as [27]:

$$\text{Rate} = \ln(C_t/C_0) = -kt \quad (2)$$

where k (min^{-1}) is the apparent pseudo-first order reaction rate constant, C_0 is absorbance of MO dye in solution at the initial stage, C_t is the absorbance at a given time and t (min) is the reaction time. Adsorption tests in dark were carried out in order to evaluate the adsorption of dye on catalyst surface and C_t/C_0 versus irradiation time was plotted for comparison.

Effects of operational parameters under visible light

Photocatalyst load and initial MO concentration

The effect of photocatalyst load, CdS//UiO-66/Ag₃PO₄ (R4), was investigated to find the optimum amount of the catalyst at which the degradation was higher that prevents excess use of photocatalyst. To this effect, the catalyst dose was varied from 0.01 to 0.4 g/L keeping other parameters such as initial dye concentration and pH constant (10 mg/L and pH 4). The effect of concentration of MO solution was studied by varying the initial MO concentration keeping pH = 4 and photocatalyst load 0.2 g/L.

Initial pH and point of zero charge (PZC)

The effect of pH of the aqueous MO solution was determined by adjusting the pH of the initial MO solution at 2, 4, 6, 8, 10 and 12 using 1, 0.1 and 0.01 M HCl and NaOH solutions each time for the optimum initial MO concentration and adsorbent dose of the photocatalyst in 100 mL of solution. The pH with higher degradation efficiency was obtained. The pH of the PZC of CdS/UiO-66/Ag₃PO₄ (R4) was determined following the procedure described in [28].

Scavengers

To evaluate the predominant active species responsible for MO degradation, photocatalytic experiments were undertaken in the presence of scavengers. To this effect, the active species such as h^+ , *O_2 and $\bullet OH$ were deliberately scavenged using scavengers NaHCO₃, AgNO₃ and methanol, respectively [29]. Typically, 0.2 g/L CdS/UiO-66/Ag₃PO₄ (R₄) (4:1) and 0.1 M of 10 mL of each scavenger were placed into 100 mL of 10 mg/L of dye solution, then, the suspension was irradiated using visible light irradiation for the same time. Then 10 mL suspension was withdrawn at 20 min interval and centrifuged at 3000 rpm for 10 min. Absorbance of the dye was determined using UV/Visible spectrophotometer at the λ_{max} of MO solution. Finally, the degradation efficiency of the photocatalyst over the dye was calculated to evaluate the main role of active species.

Real sample

The wastewater collected from Bahir Dar Textile Share Company was treated using ternary CdS /UiO-66/Ag₃PO₄ (R₄) (4:1) nanocomposite under optimized conditions upon shining visible light irradiation. The experiment was conducted by taking 100 mL of sample of wastewater in 250 mL beaker and its pH was adjusted at 4. Then 0.2 g/L of the photocatalyst was added into the solution and the suspension was kept in the dark for 1h with continuous stirring to make sure the establishment of adsorption/desorption equilibrium. Finally, the suspension was irradiated with visible light upon continuous stirring and its absorbance was measured at 20 min interval by withdrawing 10 mL suspension for 180 min. Then the plot of C_t/C_0 versus irradiation time was plotted.

RESULTS AND DISCUSSION

Characterization of the as-synthesized photocatalysts

XRD patterns. Figure 1 shows the XRD patterns of the as-synthesized UiO-66 and the corresponding hybrids with Ag_3PO_4 and CdS. For UiO-66(S_1) the intensive peaks appearing at small 2θ angles in the XRD pattern are characteristics of porous materials, which possess abundant pores or cavities. The most probable diffraction peaks of the MOFs were found below the scattering angle (2θ) of 10° and this may be due to the inverse relation of 2θ and porosity of the photocatalyst [30]. For Ag_3PO_4 (S_2), the peaks identified at 2θ equal to 33.29° , 36.57° , 55.0° , 20.87° , 29.69° , 47.79° , 52.68° , 57.2° , 61.64° , 73.86° and 89.10° represent body centered cubic structure [JCPDS:96-153-0490], which is similar with values obtained in previous reports [31-33]. The most intense peaks observed at 2θ equal to 43.77° , 26.50° , 24.91° , 28.17° , 51.91° and 52.67° , indicate the formation of the more stable phase hexagonal greenockite structure of CdS [JCPDS: 96-900-8863] [34].

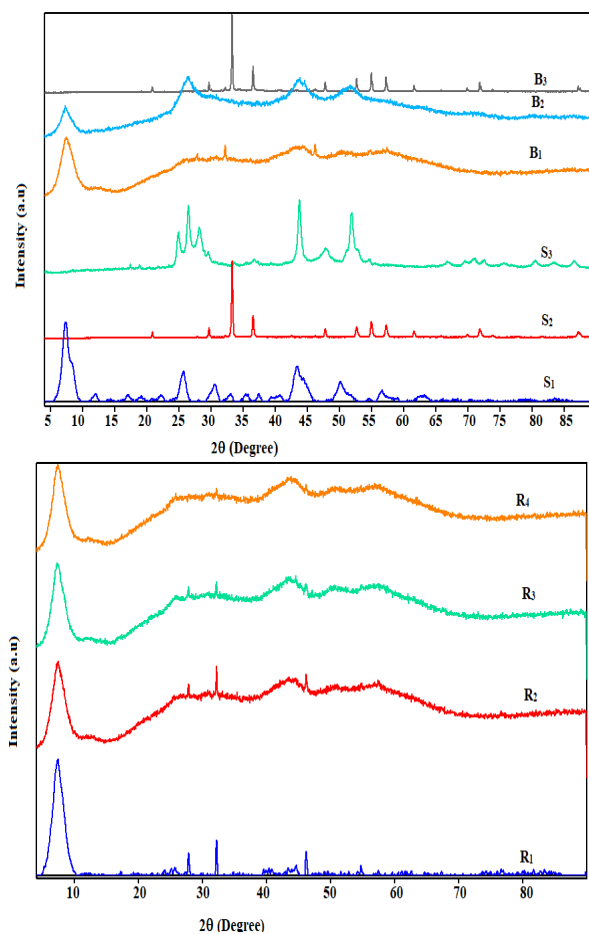


Figure 1. XRD patterns of S_1 , S_2 , S_3 , B_1 , B_2 , B_3 , R_1 , R_2 , R_3 and R_4 where, S_1 = UiO-66, S_2 = Ag_3PO_4 , S_3 = CdS, B_1 = $\text{Ag}_3\text{PO}_4/\text{UiO-66}$, B_2 = CdS/UiO-66 and B_3 = CdS/ Ag_3PO_4 , $\text{R} = (\text{CdS-UiO-66-Ag}_3\text{PO}_4)$.

UV-Vis diffuse absorption spectra. UV-Vis diffuse absorption spectroscopic data of UiO-66, Ag₃PO₄, CdS, Ag₃PO₄/UiO-66, CdS/UiO-66, Ag₃PO₄/CdS and CdS/UiO-66/Ag₃PO₄ (R₁, R₂, R₃, R₄) obtained from the plots of absorbance against wavelength are presented in Figure 2. The intercept of the tangent line on descending part of the absorption peak at the wavelength axis gives the value of absorption maximum λ_{\max} . Estimation of band gap energy using UV-Vis absorption spectroscopy in dispersed samples may not sometimes provide clear tangential line as the peak may not be well resolved for a given sample. To avoid this, we use Tauc plot of absorbance against wavelength using equation [38]:

$$\alpha h\nu = A (h\nu - E_g)^{n^2} \quad (4)$$

where α , $h\nu$, A , and E_g are optical absorption coefficient, the photonic energy, proportionality constant, and band gap energy, respectively. The direct band gaps of the prepared photocatalysts were determined from the plot of $(\alpha h\nu)^2$ vs $h\nu$ as indicated in Figure 2. The calculated band gaps of the single systems UiO-66, Ag₃PO₄ and CdS are found to be 3.45, 2.43, and 2.44 eV. These findings are similar with previous reports made on these nanoparticles [26, 39]. The binary systems Ag₃PO₄/UiO-66 (B₁), CdS/UiO-66 (B₂) and CdS/Ag₃PO₄ (B₃) have exhibited calculated band gaps of 2.6, 2.9 and 2.5 eV, respectively. The results obtained as such are in good agreement with results of the previously reported works [21, 40]. In the ternary systems R₁, R₂, R₃ and R₄, the calculated band gap energies were recorded as 2.14, 2.14, 2.13 and 2.12 eV, respectively. As can be noted here, formation of the ternary systems resulted in even lower band gaps which resulted from the interfacial combination and matched band edges formed between the three individual synthesized nanocomposite (CdS/UiO-66/Ag₃PO₄). Based on the calculated band gaps and preliminary photocatalysis result (Data not shown) R₄ was selected for further study.

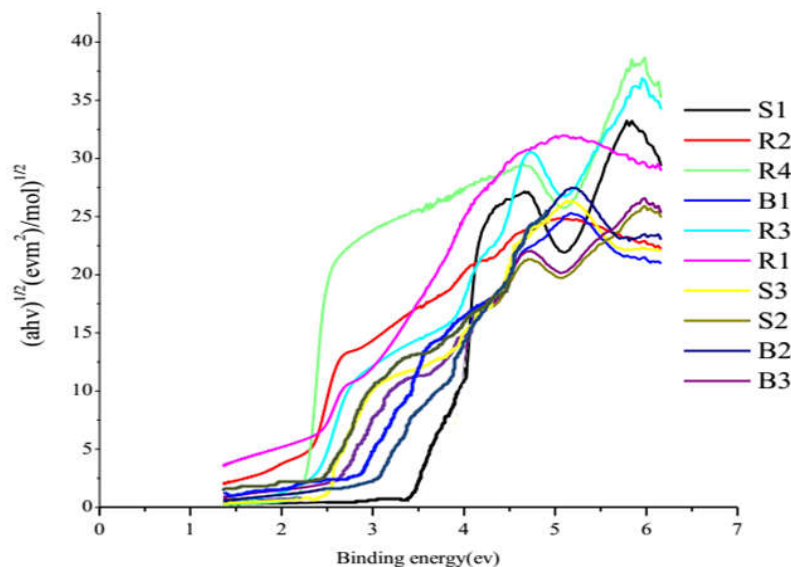


Figure 2. UV-Visible diffuse reflectance spectra of S₁, S₂, S₃, B₁, B₂, B₃, R₁, R₂, R₃ and R₄.

SEM-EDX analysis. The morphologies of the as-synthesized nanomaterials namely, UiO-66, Ag₃PO₄, CdS, Ag₃PO₄/UiO-66, CdS/UiO-66, CdS/Ag₃PO₄ and CdS/UiO-66/Ag₃PO₄ (R₁, R₂, R₃ and R₄) were characterized by SEM-EDX. Figure 3 depicted only the ternary nanocomposite

selected for photocatalytic application. Despite this, from the SEM images, one can discern that all the single and binary systems have irregular shapes with no distinct morphologies (data not shown). In contrast to this result, almost all the ternary systems appeared to be rod like structures. The elemental compositions of the as-synthesized nanomaterials were determined by EDX. The ternary systems revealed the presence of silver (0.4-6%; 0-2.7%; 0-3.4%; 0-5.6%) and zirconium (62.5-98.9%; 92.5-100%; 96.2-100%; 93.7-99.2%) for R₁, R₂, R₃ and R₄, respectively, evidencing the heterogeneity of the ternary systems.

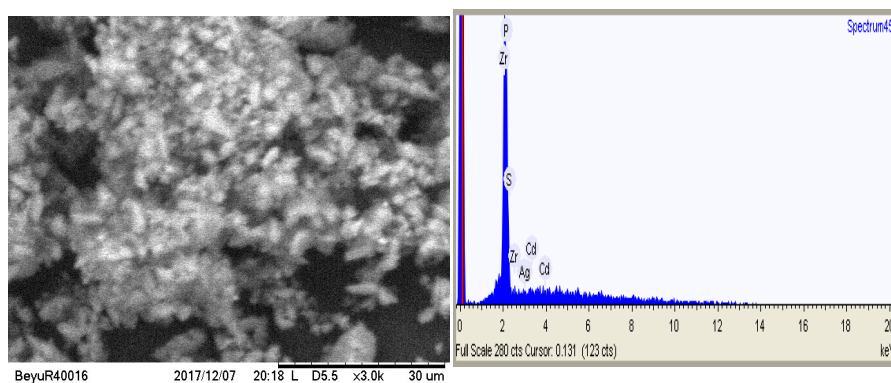


Figure 3. SEM-EDX images of the selected ternary composites R₄.

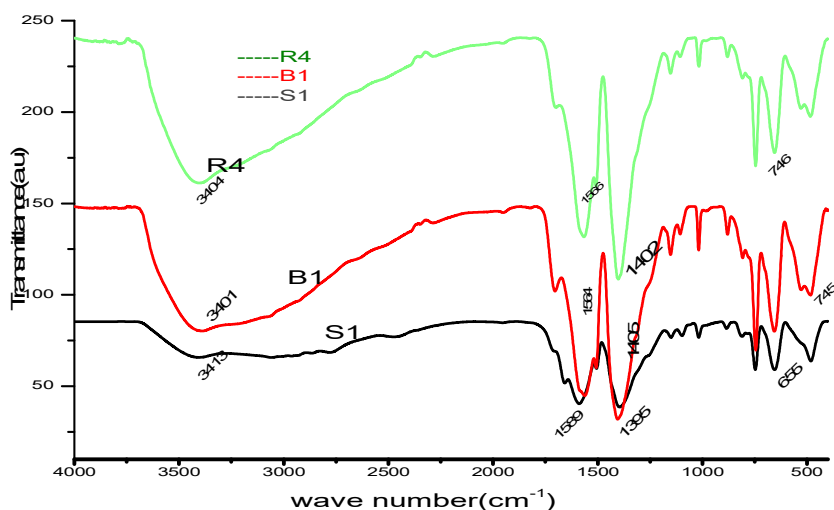


Figure 4. FTIR spectrum of synthesized nanocomposite S₁ (UiO-66), B₁ (Ag₃PO₄/UiO-66) and R₄ (CdS/Ag₃PO₄/UiO-66).

FTIR spectra. FTIR spectra in the range from 400 to 4000 cm⁻¹ was carried out to identify the surface functional groups of selected as-synthesized nanomaterials, single UiO-66(Zr) (S₁), binary Ag₃PO₄/UiO-66 (B₁) and ternary CdS/Ag₃PO₄/UiO-66 (R₄) (4:1) (Figure 4). For UiO-66, the characteristic peaks at 1589, 1566 and 1405 cm⁻¹ were assigned to the stretching vibrations

of C=O in the carboxylic acid present in H₂BDC. This band indicates existence of a coordinate bonding of the metal with the organic fraction of terephthalic acid [41]. The small bands at 1564 cm⁻¹ and 1395 cm⁻¹ represent the typical frame vibration of a benzene ring. The peaks at 746 cm⁻¹ and 655 cm⁻¹ are due to -Zr-(μ₃)O [18]. In the case of Ag₃PO₄/UiO-66 and CdS/UiO-66/Ag₃PO₄ nanocomposite, the characteristic bands for UiO-66 still remain but there is a shift in wave number in the later cases. The O-H stretching vibrations for the binary (B₁) and ternary R₄ nanocomposite were 3404 and 3401 cm⁻¹, respectively. The stretching vibration of C=O for the binary and ternary systems shift into the lower wave number compared to that of UiO-66. For UiO-66 the characteristic peaks at 1589, 1405 and 746 cm⁻¹ shift to 1564, 1402 and 745 cm⁻¹ in the case of the composites. These shifts in the characteristic peaks of UiO-66 to the lower wave numbers may be the result of the interactions between the CdS, UiO-66 and Ag₃PO₄ with nanocomposite. Shifting the peaks to lower wave number benefits the photo generated electron transfer and hence enhances the photocatalytic activity of composites. The characteristic peak at 3413 cm⁻¹ could be attributed to the O-H stretching vibration. Band at 746 cm⁻¹ can be ascribed to Cd-S stretching of synthesized nano-composite [42].

Photoluminescence (PL) study

The photoluminescence's spectra of the nanocomposite materials were shown in Figure 5. It was observed that PL intensity of the binary and ternary nanocomposites is much lower as compared to their respective single nanomaterials. Photoluminescence effect is present as the result of direct recombination, lower recombination of generated carriers causing the decrease of light emission intensity. The order of intensity is UiO-66 (S₁) > CdS (S₃) > Ag₃PO₄ (S₂) > UiO-66/CdS (B₂) > UiO-66/Ag₃PO₄ (B₁) > Ag₃PO₄/CdS (B₃) > R₁ > R₂ > R₃ > R₄. It is in good agreement with the results obtained for photocatalytic degradation curves presented in the Figure 6.

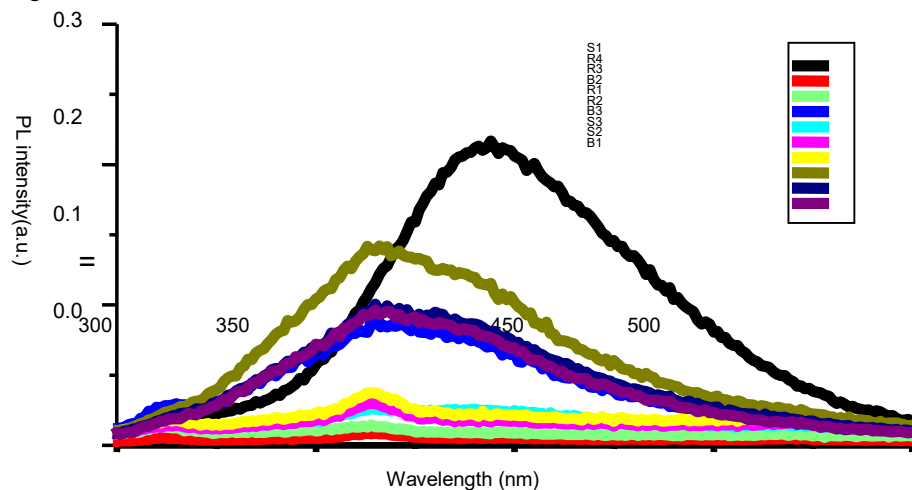


Figure 5. Photoluminescence spectra of the as-synthesized nanocomposites.

In binary and ternary nanocomposite systems the photoinduced electrons and holes can be effectively separated and hence excitonic PL intensity goes down. This is because, the lower the excitonic PL intensity, the stronger the capacity of the coupled materials to capture photo-induced electrons, the higher the separation rate of photo induced electrons and holes, and hence the higher the photocatalytic activity. It is evidently observed from photoluminescence spectra

that the ternary (R_4) nanocomposite prepared in the present work showed relatively higher efficiency for photocatalytic degradation that concurs the result obtained from XRD and UV-Vis results. This finding is also supported from the photocatalytic activity of this composite compared with its single and binary congeners.

Photocatalytic studies

Comparison of photocatalytic activities of as synthesized photocatalysts. It is known that the photocatalytic redox reaction mainly takes place on the surface of the photocatalysts and the improved surface properties significantly influence the efficiency of the photocatalysts. In this work, single, binary and ternary photocatalyst materials (UiO-66, Ag_3PO_4 , CdS, $Ag_3PO_4/UiO-66$, CdS/UiO-66, CdS/ Ag_3PO_4 and CdS/UiO-66/ Ag_3PO_4 (R_1 , R_2 , R_3 and R_4)) were synthesized by different methods. The photocatalytic activities of synthesized nanomaterials were compared using water soluble model dye (MO) solution. The highest percentage degradation registered for each of the photocatalysts namely S_1 , S_2 , S_3 , B_1 , B_2 , B_3 , R_1 , R_2 , R_3 , and R_4 were found to be 26.6, 46.7, 32.0, 46.2, 45.1, 54.0, 57.2, 66.0, 70.5 and 89.3, respectively as indicated in Figure 6.

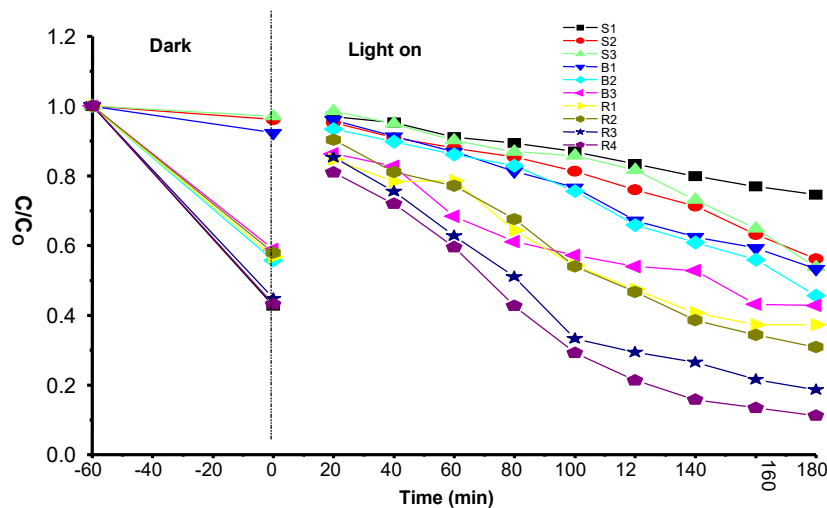


Figure 6. Comparison of photocatalytic activities of as-synthesized single, binary and ternary photocatalysts (Sorption-desorption equilibrium is done for 1 h before the photocatalysis is initiated).

In general, all the as-synthesized materials performed better as compared to the pristine MOF (UiO-66). This possibly happened as the result of poor absorption in the visible irradiation due to its wide band gap. The relatively higher photocatalytic performance of CdS and Ag_3PO_4 could possibly be due to their sensitivity to visible irradiation as evidenced in their narrow band gap. Despite this finding, the performance of Ag_3PO_4 was even better as the result of its more oxidizing valence band that involves holes in the photo-oxidation process. Contrary to the host MOF, the MOF composited with narrow band semiconductors showed better photocatalytic activities evidencing the sensitizing ability of the narrow band semiconductors in both respects. As reported by [31-33], the binary systems CdS/UiO-66, $Ag_3PO_4/UiO-66$ and CdS/ Ag_3PO_4 show higher degradation of methyl orange under visible light irradiation as compared with the

single photocatalyst UiO-66. This may be explained in terms of the possible retardation of the photochemical process due to some likely back reaction taking place between CdS or Ag₃PO₄ with UiO-66 there by producing more number of charge carriers that would consequently increase the degradation efficiency. Thus, the efficiency of photogenerated electron-hole in the binary systems CdS/UiO-66 and Ag₃PO₄/UiO-66 was higher than that of the pristine UiO-66.

When it comes to the ternary photocatalysts (CdS/UiO-66/Ag₃PO₄), they exhibit the highest photocatalytic activity compared with their binary congeners; Ag₃PO₄/UiO-66, CdS/UiO-66 and CdS/Ag₃PO₄. The pronounced enhancement of the photocatalytic activity by the ternary nanocomposites may be attributed for their having more than one paths to form electron-hole pairs because of the existence of three different interfaces, and the electron-hole recombination prevented to the maximum extent in such system. Among the ternary systems, the nanocomposite R₄ (4:1) showed highest photocatalytic activity as compared with the other percentage ratios and hence selected for the subsequent study. Enhanced photocatalytic activity of R₄ could be due to effective loading of Ag₃PO₄ and CdS on UiO-66 nanocomposite to create visible sensitive heterojunction which increases its photo absorption capacity in the visible region.

Effect of experimental parameters on MO degradation under visible light

pH_{pzc} and Effect of pH

The pH_{pzc} of the photocatalyst was found to be 5.89 (data not shown), which is expected to be the point at which the surface charge of R₄ is neutral. The photodegradation result shown below revealed that higher adsorption and higher photocatalysis were obtained at pH less than the PZC of the catalyst, which is pH = 4.0. This is due to the higher interaction between the positively charged surface of the photocatalyst particles and the negatively charged (anionic) MO molecules at this pH. To study the effect of pH on the degradation of MO, the experiments were carried out at various pH values, ranging from 2 to 12 by adjusting with 0.1 M each of NaOH or HCl, the catalyst load 0.2 g/L and at 10 mg/L dye concentration (Figure 7).

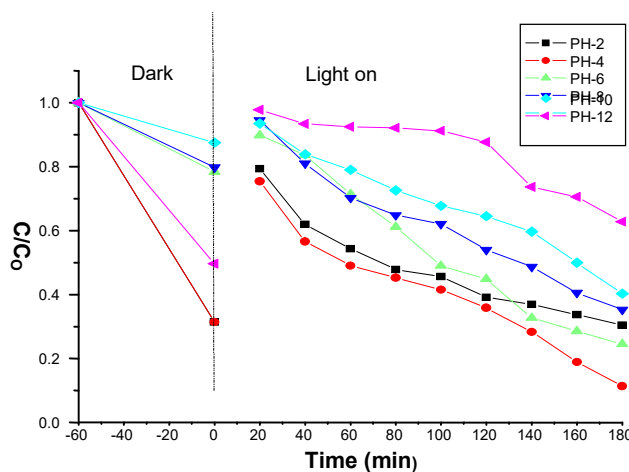


Figure 7. The effect of pH on the degradation of MO as function of irradiation time with a catalyst loading of 0.2 g/L and concentration of MO of 10 mg/L under visible-light (sorption-desorption equilibrium is done 1 h before the photocatalysis is initiated).

The percent degradation increased considerably with an increase in pH from 2 to 4 for as-synthesized nanocomposite and this indicates the percentage decolorization/degradation is higher at acidic condition than the alkaline condition. The photocatalyst exhibited maximum rate of degradation (90%) at pH = 4 at 180 min. Unlike others, the percent degradation declined beyond this pH. The general trend is, however, similar to previous studies done for photocatalytic degradation of MO dyes [43, 44].

Effect of initial dye concentration

The photocatalytic degradation of dye was carried out by varying the initial concentration of dye from 10 to 30 mg/L in order to determine the appropriate dose of dye solution. It was found that nanocomposites exhibited a higher photocatalytic activity at a low dye concentration (10 mg/L) but showed decreased degradation efficiency at high initial dye concentration (data not shown). This is because with increase in the dye concentration, the solution becomes more intense in color and the path length of the photons entering the solution is decreased resulting in only a few photons reaching the catalyst surface. Hence, the productions of hydroxyl radicals are reduced. Therefore, the degradation efficiency is reduced [45]. This negative effect is because of the following reasons: the number of dye molecules that are adsorbed on the surface of photocatalyst increase because of the increment in dye concentration. In addition, at a high dye (MO) concentration a significant amount of visible light is absorbed by the dye molecules [46]. The generation of OH[·] radicals on the surface of catalyst is likely to be reduced since active sites on the surface of the catalyst are occupied by the dye ions.

Effect of photocatalyst loading

Influence of photocatalyst dose on the degradation of organic pollutants was carried out by varying the catalyst dose from 0.01 to 0.4 g/L (Figure 8). In this study, the degradation of MO initially increases with increasing in photocatalyst load from 0.01 g/L to 0.2 g/L. However, further increase of the catalyst loading from 0.2 g/L to 0.4 g/L results in decreased the degradation of MO. This may be due to non uniform light intensity distribution apparently resulting from overloading. As the result, the reaction rate would become lower with increased photocatalyst dosage. At the same time, at lower photocatalyst loading, the degradation of the organic molecule; (MO) should be lower implying that more light is transmitted through the reactor and lesser transmitted radiation would only be utilized in the photocatalytic reaction [47]. The optimum catalyst dose for synthesized nanocomposite was found to be 0.2 g/L. The result was similar to that of [44], who demonstrated that the effect of catalyst loading would be more on the solar photocatalytic degradation for the range 0.01 to 0.4 g/L of MO. A number of studies have indicated that the photocatalytic degradation rate initially increased with catalyst loading and then decreases at higher values because of light scattering and screening effects. The tendency towards agglomeration (particle-particle interaction) also increases at high solids concentration, resulting in a reduction in catalyst surface area available for light absorption and hence a drop in the photocatalytic degradation rate. Although the number of active sites in solution will increase with catalyst loading, a point appears to be reached where light penetration is to be compromised because of excessive particle concentration. The trade off between these two opposing phenomena results in an optimum catalyst loading for the photocatalytic reaction [48].

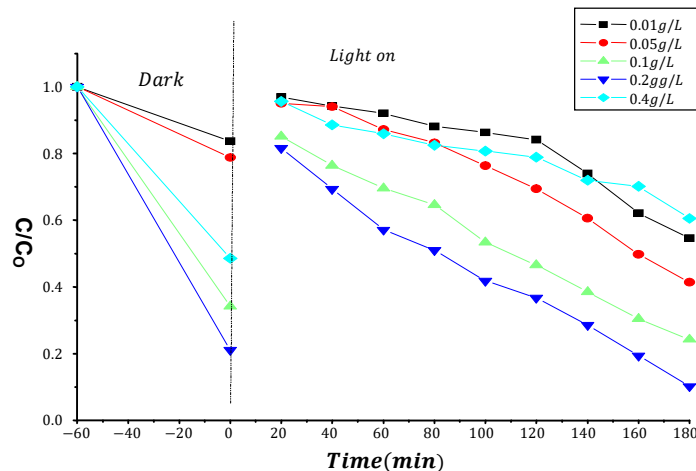


Figure 8. The effect of catalyst loading on photocatalytic activities of as synthesized nanocomposite with respect to irradiation time (sorption-desorption equilibrium is done or 1 h before the photocatalysis is initiated).

Effect of scavengers

To evaluate the mechanism of photocatalytic degradation of CdS/UiO-66/Ag₃PO₄ (R4) over methyl orange, the influences of active species such as superoxide radical ($^{\cdot}\text{O}_2^-$), hole (h^+) and hydroxyl radical ($^{\cdot}\text{OH}$) on the photo degradation process were evaluated using 10 mg/L of MO and 0.2 g/L of the photocatalyst at pH = 4 (Figure 9). Different scavengers were used to remove the corresponding active species so that the function of different active species in the photocatalytic activities process based on the change of photocatalytic conversion of targeted pollutant methyl orange could be understood. The scavengers used in this reaction were NaHCO₃ for h^+ , CH₃OH/H₂O for $^{\cdot}\text{OH}$ and AgNO₃ for superoxide radical $^{\cdot}\text{O}_2^-$ [49]. The photocatalytic conversion of MO without scavenger was 88.2%. When AgNO₃ was added, the photocatalytic degradation of MO decreased to 63% where as when CH₃OH/H₂O and NaHCO₃ were added, the photocatalytic conversion of MO become 64.8% and 74.08%, respectively. The results indicated that all the scavengers considered have suppressed the photocatalytic degradation efficiency of the photocatalyst although the effect of AgNO₃ and CH₃OH/H₂O are more pronounced. Therefore, the main active species in this photo degradation reaction are the superoxide radical $^{\cdot}\text{O}_2^-$ and hydroxyl radicals. The direct involvement of holes appeared to be restricted. Rather the holes involve indirectly via the reaction of these species with water molecules to create very reactive hydroxyl radicals. This experiment evidences the involvement of the conduction band electrons and the valence band holes in the redox process with the highest photocatalytic efficiency observed with the ternary systems as compared with their binary congeners.

Analysis of real sample

The efficiency of the as-synthesized R₄ photocatalyst was studied on the degradation of the real sample under visible light irradiation by using 0.2 g/L photocatalyst load at pH = 4, whose result is shown in Figure 10. The degradation efficiency in the real wastewater sample which was 71.22% found to be lower than that of the model MO solution (90%) due to the complexity of

the wastewater which includes not only mixture of organic dyes but also other chemicals from the bleaching steps [50].

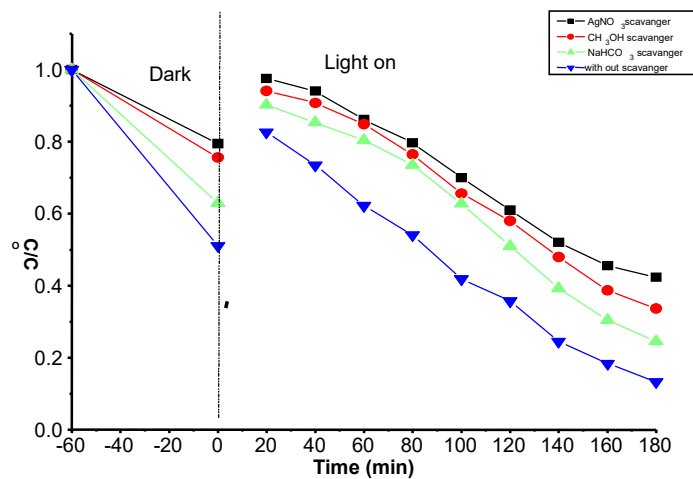


Figure 9. Degradation rate of MO as function of irradiation time in the absence and presence of scavengers (sorption-desorption equilibrium is done 1 h before the photocatalysis is initiated).

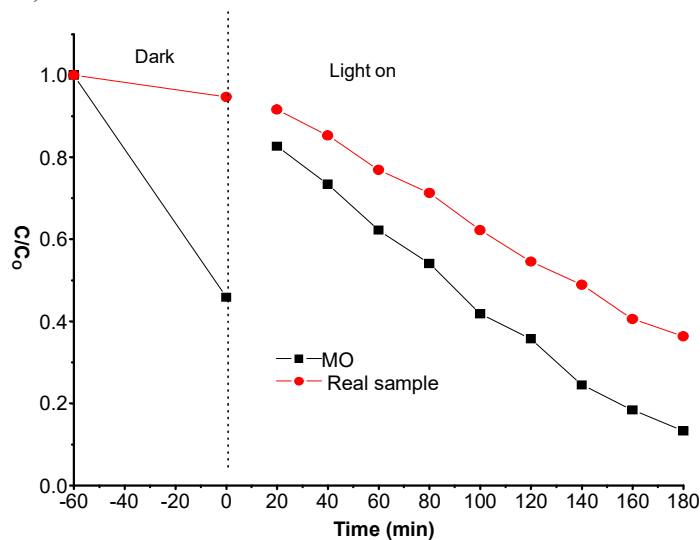


Figure 10. Photocatalytic degradation of MO and real textile wastewater using R₄ (sorption-desorption equilibrium is done for 1 h before the photocatalysis is initiated).

CONCLUSION

The crystal structures, band gaps, surface morphology, thermal stability, bond vibration (stretching), optical properties and specific surface area of all nano-composite were studied

using XRD, UV-Vis, SEM-EDX, FTIR and PL analytical techniques, respectively. The study examined in detail the effect of key parameters, such as catalysts loading, pH, concentration of dye, point of zero charge and optimization of ternary loading for the degradation of MO dye under UV-Vis light irradiation. Photocatalytic degradation activity of the nanocomposite under visible light irradiation has been evaluated for model pollutant MO dye solution as well as on real sewage sample collected from Bahir Dar Textile Share Company. Results suggested that the optimization of ternary CdS/UiO-66/Ag₃PO₄ (R₄) nanocomposite photocatalyst exhibited a relatively higher efficiency on the degradation of both MO and real sewage sample which are about 90% and 71.2%, respectively. All the results confirmed that the photocatalytic degradation of optimize ternary, R₄ (CdS/UiO-66/Ag₃PO₄) system was comparatively higher than its ternary (R₁, R₂, R₃), binary and single forms.

ACKNOWLEDGEMENTS

The authors would like to acknowledge the financial support received from Ministry of Education through Office of the Research and Extension V/President, Haramaya University. The support in characterizing our samples received from Instituto de Catalisis y Petroleoquimica, CSIC, via a project code (HURG-2016-03-02) is also highly acknowledged.

REFERENCES

1. Wang, H.; Zhang, L.; Chen, Z.; Hu, J.; Li, S.; Wang, Z.; Liu, J.; Wang, X. Semiconductor heterojunction photocatalysts: Design, construction, and photocatalytic performances. *Chem. Soc. Rev.* **2014**, 43, 5234-5244.
2. Rashed, M.N.; El-Amin, A.A. Photocatalytic degradation of methyl orange in aqueous TiO₂ under different solar irradiation sources. *Int. J. Phys. Sci.* **2007**, 2, 73-81.
3. Pelizzetti, E.; Serpone, N. *Homogeneous and Heterogeneous Photocatalysis*. Reidel Publishing Company: Dordrecht, Holland; **1985**; p 720.
4. Vakiti, R.J. Hydro/solvothermal synthesis, structures of metal-organic frameworks based on s-block metals. Masters Theses and Specialist Project, Western Kentucky University, Bowling Green, Kentucky, **2012**.
5. Agarwal, K. Removal of dyes using conventional and advanced adsorbents. B. Tech. Project Report, National Institute of Technology Rourkela, India, **2013**.
6. Hoffmann, M.R.; Martin, S.T.; Choi, W.; Bahnemann, D.W. Environmental applications of semiconductor photocatalysis. *Chem. Rev.* **1995**, 95, 69-96.
7. Amogne, W.Y.; Belete, B.B.; Shimelis, A.; Tadesse, A.M. MWCNTs/Ag-ZnO nanocomposite for efficient photocatalytic degradation of Congo red. *Bull. Chem. Soc. Ethiop.* **2020**, 34, 55-66.
8. Chong, M.N.; Jin, B.; Chow, C.W.K.; Saint, C. Recent developments in photocatalytic water treatment technology: A review. *Water Res.* **2010**, 44, 2997-3027.
9. Asahi, R.T.; Morikawa, T.; Ohwaki, T.; Aoki, K.; Taga, Y. Visible-light photocatalysis in nitrogen-doped titanium oxides. *Science* **2001**, 293, 269-271.
10. Wang, Y.; Wang, Q.; Zhan, X.; Wang, F.; Safdar, M.; He, J. Visible light driven type II heterostructures and their enhanced photocatalysis properties: A review. *Nanoscale* **2013**, 5, 8326-8339.
11. Wang, W.; Cheng, B.; Yu, J.; Liu, G.; Fan, W. Visible-light photocatalytic activity and deactivation mechanism of Ag₃PO₄ spherical particles. *Chem. Asian J.* **2012**, 7, 1902-1908.
12. Mohanty, R.P. Fabrication and characterization of metal-organic framework (MOF) based membrane. B. Tech Project, National Institute of Technology, Rourkela, India, **2012**.

13. Zaho, X.; Wang, Y.; Dong-Sheng L. Metal-organic frameworks for separations. *Adv. Mater.* **2018**, *30*, 1705189.
14. Zhang, T.; Webin, L. Metal-organic frameworks for artificial photosynthesis and photocatalysts. *Chem. Soc. Rev.* **2014**, *43*, 5982-5993.
15. Zhu, J.F. New photocatalysts based on MIL-53 MOFs for the decolorization of methylene blue dye. *J. Hazard. Mater.* **2011**, *190*, 945-951.
16. Wang, Y.; Xiuli, Y.W.; Caimei, F. Novel visible-light AgBr/Ag₃PO₄ hybrids photocatalysts with surface plasma resonance effects. *J. Solid State Chem.* **2013**, *9*, 311-330.
17. Li, R.; Hu, J.; Deng, M.; Wang, H.; Wang, X.; Hu, Y.; Jiang, H.L.; Jiang, J.; Zhang, Q.; Xie, Y.; Xiong, Y. Integration of an inorganic semiconductor with a metal-organic framework: A platform for enhanced gaseous photocatalytic reactions. *Adva. Mater.* **2014**, *26*, 4783-4788.
18. Cavka, J.; Olsbye, U.N.; Guillou, C.; Lamberti, S.B.; Lillerud, K.P. A new zirconium inorganic building brick forming metal organic frameworks with exceptional stability. *J. Am. Chem. Soc.* **2008**, *130*, 13850-13851.
19. Zhang, W.; Lu, G.; Cui, C.; Liu, Y.; Li, S.; Yan, W.; Xing, C.; Chi, Y.R.; Yang, Y.; Huo, F. A family of metal-organic frameworks exhibiting size-selective catalysis with encapsulated noble-metal nanoparticles. *Adv. Mater.* **2014**, *26*, 4056.
20. Sha, Z.; Chan, H.S.; Wua, J. Ag₂CO₃/UiO-66(Zr) composite with enhanced visible-light promoted photocatalytic activity for dye degradation. *J. Hazard. Mater.* **2015**, *299*, 132-140.
21. Zhou, J.J.; Wanga, R.; Liua, X.L.; Penga, F.M.; Lia, C.H.; Teng, F.; Yuan, Y.P. In situ growth of CdS nanoparticles on UiO-66 metal-organic framework octahedrons for enhanced photocatalytic hydrogen production under visible light irradiation. *Appl. Surf. Sci.* **2015**, *346*, 278-283.
22. Silva, G.C.; Luz, I.; Francese X., Corma, A. and Garcia, H. Water stable zirconium benzenedicarboxylate metal-organic frameworks as photocatalysts for hydrogen generation. *Chem. Eur. J.* **2010**, *16*, 11133-11138.
23. Bi, Y.; Ouyang, S.; Cao, J.; Ye J. Facile synthesis of rhombic dodecahedral AgX/Ag₃PO₄ (X = Cl, Br, I) heterocrystals with enhanced photocatalytic properties and Stabilities. *Phys. Chem.* **2011**, *13*, 10071-10075.
24. Singh, V.; Sharma, P.; Chauhan, P. Synthesis of CdS nanoparticles with enhanced optical properties. *Mater. Charact.* **2011**, *62*, 43-52.
25. Jo, Z.K.; Kim, I.Y.; Lee, J.M.; Nahm, S.; Choi, J.W.; Hwang, S.J. Surface-anchored CdS-Ag₃PO₄ nanocomposite with efficient visible light photocatalytic activity. *Mater. Lett.* **2014**, *114*, 152-155.
26. Zhao, X., Liu, X., Zhang, Z., Liu, X. and Zhang. Facile preparation of a novel SnO₂/UiO-66/rGO hybrid with enhanced photocatalytic activity under visible light. *RSC Adv.* **2016**, *6*, 92011-92019.
27. Kaur, S.; Singh, V. TiO₂ mediated photocatalytic degradation studies of reactive red by UV irradiation. *J. Hazard. Mater.* **2007**, *141*, 230-236.
28. Panumati, S.; Chudecha, K.; Vankhaew, P. Adsorption of phenol from diluted aqueous solutions by activated carbons obtained from bagasse, oil palm shell and pericarp of rubber fruit. *J. Sci. Technol.* **2008**, *30*, 185-189.
29. Qamar, M.; Saquib, M.; Muneer, M. Titanium dioxide mediated photocatalytic degradation of two selected azo dye derivatives, chrysoidine R and acid red 29 (chromo trope 2R), in aqueous suspensions. *Desalination* **2005**, *186*, 255-271.
30. Lin, K.S.; Adhikari, A.K.; Su, Y.H.; Chiang, C.L.; Dehvari, K. Structural characterization of chromium atoms in MIL-101 metal organic framework using XANES/EXAFS spectroscopy. *Chin. J. Phys.* **2012**, *50*, 322-331.

31. Girma, T. Zeolite supported Ag₃PO₄-ZnO-Fe₂O₃ nanocomposite: Synthesis, characterization and study of its photocatalytic activity towards the degradation of methyl orange, MSc Thesis, Haramaya University, Haramaya, **2015**.
32. Anjejo, G. Zeolite supported CdS/ZnO/Ag₃PO₄ nano composite: Synthesis, characterization and photocatalytic activity for the degradation of methylene blue. MSc Thesis, Haramaya University, Haramaya, **2017**.
33. Hadush, A. Synthesis and characterization of rGO/UiO-66/Ag₃PO₄ nanocomposite for photocatalytic degradation of methyl orange. MSc Thesis, Haramaya University, Haramaya, **2018**.
34. Zhang, X.; Zhang, N.; Xu, Y.; Tang, Z.R. One-dimensional CdS-CeO₂ composites with boosted photocatalytic activity. *New J. Chem.* **2015**, 39, 6756-6764.
35. He, J.; Wang, J.; Chen, Y.; Zhang, J.; Duan, D.; Wang, Y.; Yan, Z. A dye-sensitized Pt/UiO-66 (Zr) metal-organic framework for visible-light photocatalytic hydrogen production. *Chem. Commun.* **2014**, 50, 7063-7066.
36. Endashaw, M. Synthesis and characterization of selected metal organic frameworks for photocatalytic degradation of methyl orange, Haramaya University, Haramaya, **2015**.
37. Girma, T. Synthesis and characterization of UiO-66 metal organic frameworks for simultaneous sorption of methyl orange and methylene blue from aqueous solution. MSc Thesis, Haramaya University, Haramaya, **2016**.
38. Cao, J.; Luo, B.D.; Lin, H.L.; Xu, B.S.; Chen, S. Aluminum salt slag characterization and utilization. *J. Hazard. Mater.* **2012**, 217-218, 58-66.
39. Pandey, A.; Chakrabarty, R.K.; Liu, L.; Mishchenko, M.I. Empirical relationships between optical properties and equivalent diameters of fractal soot aggregates at 550 nm wavelength. *Optics Exp. Res.* **2015**, 23, 1354-1362.
40. Jishan, W.; Hardy, S.; Zhou, S. Ag₂CO₃/UiO-66(Zr) composite with enhanced visible-light promoted photocatalytic activity for dye degradation. *J. Hazard. Mater.* **2015**, 299, 132-140.
41. Yang, P.; Liu, Q.; Liu, J.; Zhang, H.; Li, Z.; Li, R.; Liu, L.; Wang, J. Interfacial growth of a metal-organic framework (UiO-66) on functionalized graphene oxide (GO) as a suitable seawater adsorbent for extraction of uranium (VI). *J. Mater. Chem. A* **2017**, 5, 17933-17942.
42. Yang, J.; Wang, J.; Xie, L.; Jiang, Y.; Shi, F.; Yuan, F.; Yu, Sun, Y. Significantly enhanced photocatalytic hydrogen evolution under visible light over CdS embedded on metal-organic frameworks. *Chem. Commun.* **2013**, 49, 6761-6763.
43. Saleh, R.; Djaja, N.F. UV-light photocatalytic degradation of organic dyes with Fe-doped ZnO nanoparticles. *Superlatt. Microstruc.* **2014**, 74, 217-233.
44. Xiao, Q.; Zhang, J.; Xiao, C.; Si, Z.; Tan, X. Solar photocatalytic degradation of methylene blue in carbon-doped TiO₂ nanoparticles suspension. *Solar Energy* **2008**, 82, 706-713.
45. Wetchakuna, K.; Wetchakunb, N.; Sakulsermsuk, S. An overview of solar/visible light-driven heterogeneous photocatalysis for water purification: TiO₂- and ZnO-based photocatalysts used in suspension photoreactors. *J. Ind. Eng. Chem.* **2019**, 71, 19-49.
46. Alireza, K.; Reza, D.; Cheshmeh, S.; Atefeh, K. Sang, W.J. Sonocatalytic degradation of a textile dye over Gd-doped ZnO nanoparticles synthesized through sonochemical process. *Ultrason. Sonochem.* **2015**, 23, 219-230.
47. Neppolian, B.; Choi, H.; Sakthivel, S.; Arabindoo, B.; Murugesan, V. Solar-induced photocatalytic degradation of three commercial textile dyes. *J. Hazard. Mater.* **2002**, 89, 303-317.
48. Adesina, A.A. Industrial exploitation of photocatalysis: Progress, perspectives and prospects. *Catal. Survey Asia* **2004**, 8, 265-273.
49. Liu, W.; Wanga, M.; Xu, C.; Chen, S.; Fu, X. Ag₃PO₄/ZnO: An efficient visible light sensitized composite with its application in photocatalytic degradation of rhodamine B. *Mater. Res. Bull.* **2013**, 48, 106-113.

50. Kiros, G.; Mayoral, A.; Marquez-Alvarez, C.; Yonas, C.; Díaz, I. Enhanced photocatalytic activity of TiO₂ supported on zeolites tested in real waste waters from the textile industry of Ethiopia. *J. Micropor. Mesopor. Mater.* **2016**, *225*, 88-97.